Acta Oceanol. Sin., 2017, Vol. 36, No. 9, P. 10–14
DOI: 10.1007/s13131-017-1105-0
http://www.hyxb.org.cn
E-mail: hyxbe@263.net

The Rhines effect on the geographical characteristics of altimeter-observed eddies

LIU Zhiliang[1, 2*], PANG Chongguang[1, 2]

[1] Key Laboratory of Ocean Circulation and Waves, Institute of Oceanology, Chinese Academy of Sciences, Qingdao 266071, China

[2] Qingdao National Laboratory for Marine Science and Technology, Qingdao 266237, China

Received 13 February 2017; accepted 5 April 2017

Abstract

The Rhines effect may be regarded as an interaction between Rossby waves and turbulence, in which the Rossby waves may radiate away eddy energy when their frequencies are equal or larger than those of the turbulence, thereby deforming and eventually destroying the existing eddies. Through comparing eddy-scale velocity and long Rossby wave phase speed in the oceans, a generalized form of the Rhines effect is examined on the geographical characteristics of altimeter-observed eddies. The results show that the generalized Rhines effect has a much greater influence on eddy characteristics than its classical form, which only considers the simple beta effect due to the meridional gradient of planetary vorticity. The largest amount of eddies are detected in regions where eddy-scale velocity is larger than the critical Rossby-wave phase speed considering a generalized beta effect. The eddies in those regions can grow via an inverse kinetic energy cascade and have much larger amplitudes and sizes. The "eddy desert" regions outside of the tropical oceans, which have far fewer detected eddies and much weaker eddy amplitudes, lie in areas where the eddy-scale velocity is less than the critical Rossby-wave phase speed. In those regions, the generalized Rhines effect may be a possible mechanism of suppressing eddy growth.

Key words: Rhines effect, mesoscale eddy, Rossby wave, energy cascade, eddy desert

Citation: Liu Zhiliang, Pang Chongguang. 2017. The Rhines effect on the geographical characteristics of altimeter-observed eddies. Acta Oceanologica Sinica, 36(9): 10–14, doi: 10.1007/s13131-017-1105-0

1 Introduction

Mesoscale eddies are dominant in the mid-latitude oceans and play an important role in determining large-scale ocean circulation. On the basis of long-period, high-resolution, merged sea surface height (SSH) altimeter data, mesoscale eddies and their variability can be well identified and quantitatively analyzed (Chelton et al., 2007, 2011). Interestingly, the geographical distribution of eddies shows that there are several "eddy deserts" in the global oceans, including regions centered at approximately 50°N, 160°W in the Northeast Pacific and at approximately 50°S, 95°W in the Southeast Pacific. Furthermore, there are very few eddies in areas near 20°S (also 20°N), 20°W in the Atlantic Ocean. Meanwhile, eddy-rich regions can be found in the northwest North Pacific Ocean, the west North Atlantic Ocean, the Indian Ocean, and in the vicinity of the ACC (Antarctic Circumpolar Current) regions.

Previous studies have shown that baroclinic instability may be the primary mechanism of eddy generation (Gill et al., 1974; Stammer and Wunsch, 1999; Ferrari and Wunsch, 2009). The results of Smith (2007) and Tulloch et al. (2011) show that almost all of the global oceans are baroclinically unstable. Thus, the eddies may exist in eddy-poor regions, but with magnitudes too small to be resolved by SSH signals. The question then arises as to why the eddies in the eddy-poor regions cannot grow as large as those in the eddy-rich regions.

As we know, an inverse kinetic energy (KE) cascade may supply the energy to ocean eddies for their growth via "triad interactions" (Scott and Wang, 2005; Qiu et al., 2014; Sasaki et al., 2014; Wang et al., 2015). The fact that no eddies in the "eddy deserts" are large enough to be resolved by altimeter data suggests that there may be a mechanism that suppresses the inverse cascade, which could prevent eddies from growing. According to the classical baroclinic instability theory (Charney, 1947; Eady, 1949; Phillips, 1954; Smith, 2007; Tulloch et al., 2011), the fastest mode of the baroclinic instability occurs near the scale of the first baroclinic Rossby radius of deformation. If there is a sufficient scale separation between the Rhines scale and the Rossby radius, an inverse KE cascade could occur, which may supply energy for the eddy growth (Vallis and Maltrud, 1993; Scott and Wang, 2005; Chemke and Kaspi, 2015). The Rhines scale, $L_{\mathrm{R}} = \left(\frac{2U}{\beta}\right)^{1/2}$, where U is a root-mean-square (RMS) fluid velocity, and β is the meridional derivative of the Coriolis parameter, has been proved to significantly affect the eddy growth during the interaction between turbulence and waves, either in barotropic flows (Rhines, 1975; Sukoriansky et al., 2007; Chemke and Kaspi, 2015, 2016) or in baroclinic cases (Smith, 2004; Theiss, 2006; Tulloch et al., 2009). At this scale, the inverse cascade supposedly becomes

Foundation item: The National Natural Science Foundation of China under contract No. 41276026; the Ocean Strategic Pilot Project of Chinese Academy of Sciences under contract No. XDA11020301; the Key Program of National Natural Science Foundation of China under contract No. 61233013.

*Corresponding author, E-mail: zhlliu@qdio.ac.cn

arrested, and the nonlinear turbulence will be replaced by the excitation of linear Rossby waves. Thus, when the eddies grow large to the Rhines scale via inverse KE cascade, the eddy energy may be radiated away as excited Rossby waves and the inverse cascade may slow down, which leads the eddies cease growing. This wave-turbulence interaction, which have obvious influence on eddy growth, is refered to as the "Rhines effect" (Williams, 1978; Theiss, 2006; Tulloch et al., 2009). Recently, Wang et al. (2015) determined the global distribution of the largest inverse KE cascades based on SSH data, and showed that the magnitudes of the inverse cascades were extremely weak in the "eddy desert" areas but much stronger in the eddy-rich regions.

Theiss (2006) previously proposed a generalized Rhines effect, in which a baroclinic zonal mean current and its meridional shear were taken into account, and applied it to the observed storms on Jupiter. He found that most of the observed storms occurred in regions of U_e>U_{cg}, where U_e is the eddy scale velocity and U_{cg} is the critical Rossby-wave phase speed considering the generalized beta effect. Motivated by his results, here we examine the Rhines effect on the geographical characteristics of altimeter-observed eddies in the earth's oceans, with specific attention to the formation of oceanic "eddy deserts". Tulloch et al. (2009) also attempted to interpret the westward propagation characteristics of altimeter-observed eddies in terms of the interaction between turbulence and waves, and they argued that at higher latitude, the turbulence cannot readily excite waves because of the weak overlap in time scales between turbulence and waves. It implicitly indicates that the roles of the Rhines effect may be weak in higher latitude oceans. Here we will show that in those regions, the Rhines effect may still play crucial roles in determining the horizontal eddy scale if we consider a generalized form.

This paper is organized as follows. In Section 2, we will present the geographical distribution of scale separation between the baroclinic Rhines scale and the first baroclinic Rossby radius, which is very important for occurring of the KE inverse cascade. In Section 3, we will compare effects of the classical Rhines effect and the generalized one on the geographical distribution of the altimeter-observed eddies. Finally, we conclude with a discussion in Section 4.

2 Scale separation between baroclinic Rhines scale and first baroclinic Rossby radius

There are various methods to estimate the RMS fluid velocity U (Theiss, 2006; Tulloch et al., 2009; Chemke and Kaspi, 2015; Luo et al., 2015). Here, in order to calculate the Rhines scale, we will estimate it as the square root of the eddy kinetic energy and denote it as

$$U_e = \sqrt{u'^2 + v'^2}\ , \tag{1}$$

where (u', v') are the surface geostrophic velocity anomalies provided by SSALTO/DUACS and AVISO. Here, following Theiss (2006), we call U_e as the eddy-scale velocity.

Hence, the Rhines scale can be calculated as

$$L_R = \left(\frac{2U_e}{\beta}\right)^{1/2}. \tag{2}$$

The geostrophic velocity anomaly data constructed by SSALTO/DUACS merged all available satellite altimeter SSH measurements for the period from October 1992 to December 2015 and was interpolated onto a globally uniform (1/4)° grid with a 7 d interval. The merged product enables much better detection of mesoscale signals than a single satellite (Pascual et al., 2006; Chelton et al., 2007, 2011). It should be noted that the geostrophic velocity anomaly data may be not accurate near the equatorial regions because of the assumed geostrophic balance used in the velocity calculation.

As discussed by Tulloch et al. (2009), the surface geostrophic velocity anomalies are primarily first baroclinic in the regions away from the equator according to the results of Wunsch (1997). Consequently, the Rhines scales we estimated here are also primarily first baroclinic as Theiss (2006) did. We will further examine the scale separation between the calculated baroclinic Rhines scale and the first baroclinic Rossby radius, which is important for occurring of the inverse KE cascade.

The global first baroclinic Rossby radius (L_d) in the oceans has been determined and analyzed by several studies, including Stammer (1997), Chelton et al. (1998), and Smith (2007). Here, we use the Rossby radius data calculated by Chelton et al. (1998) to estimate the scale separation between the Rhines scale and the first baroclinic Rossby radius.

Owing to the dependence of the Rhines scale on the EKE field, the global pattern of the Rhines scale (Fig. 1a) is very similar to that of the EKE field shown by Ferrara and Wunsch (2009) and Wang et al. (2015). The largest Rhines scale values lie in the strongest EKE region, such as the vicinity of the Kuroshio Extension, the Gulf Stream extension, and the ACC region, with scales of 100–250 km. The smallest values lies in the regions of weak EKE areas, such as the northeastern North Pacific, the eastern South Pacific, the oceans around New Zealand Island, and the majority of the low latitude Atlantic, with scales smaller than 50 km. The "eddy desert" regions in the Pacific, first reported by Chelton et al. (2007), appear to belong to those areas with the smallest Rhines scales. The standard-deviation (SD) values of the calculated Rhines scales are also shown in Fig. 1, which indicate that the regions with larger Rhines scale values also have larger variance, and vice versa. The bottom panel of Fig. 1 shows the scale separation between the calculated Rhines scale and the first Rossby radius of deformation. In most tropical regions (20°S–20°N), the Rhines scales are smaller than the first baroclinic radi-

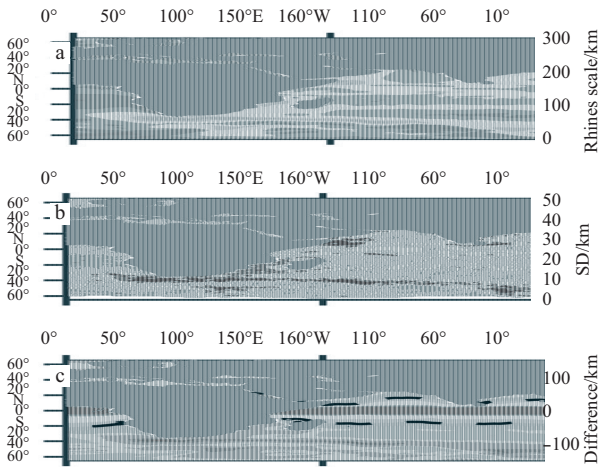

Fig. 1. The global distributions of the baroclinic Rhines scale (a), the standard deviations of the calculated Rhines scale (b), and the difference between the baroclinic Rhines scale and the first baroclinic Rossby radius (c). The dashed blank lines in the bottom panel denote 0 isolines.

us, where linear Rossby waves are dominant (Theiss, 2004, 2006; Tulloch et al., 2009). Poleward of 20°, the Rhines scales are larger than the deformation radius, and the scale separation is sufficient for an inverse KE cascade. In those areas, the spatial patterns of both the Rhines scale and the scale separation are similar to those of the geographical distribution of altimeter-observed eddy numbers and amplitude shown by Chelton et al. (2007) and Chelton et al. (2011). For example, the "eddy desert" areas reported by Chelton et al. (2007) have the smallest Rhines scale and a very short separation scale. These features imply that the Rhines effect may have a significant influence on the geographical eddy distribution, which we will further study in the next section.

3 Rhines effect on the geographical characteristics of altimeter-observed eddies

As mentioned above, the Rhines effect may be regarded as an interaction between Rossby waves and turbulence (eddies), in which the Rossby waves may radiate away eddy energy when their frequencies are equal or larger than those of the turbulence (eddies), thereby deforming and eventually destroying the existing eddies. According to the central idea of the Rhines effect, if we consider an eddy scale velocity U_e and a classical Rossby-wave phase speed U_c (here we use U_c which only considers the classical beta effect to distinguish from U_{cg} which denotes a generalized form), when $U_e \leqslant U_c$, the existing eddies could be deformed and destroyed by the Rossby waves, transferring energy to the waves (Theiss, 2006; Tulloch et al., 2009). On the other hand, when $U_e > U_c$, geostrophic eddies may continue to develop and grow to L_R from its generation scale (near L_d according to the linear baroclinic instability theory) via inverse KE cascade until the upscale-transferred energy is arrested (e.g., Rhines, 1975; Holloway and Hendershott, 1977; Galperin et al., 2006, 2010). Hence, in this section we will examine the Rhines effect on the geographical characteristics of the altimeter-observed eddies by comparing the eddy scale velocity U_e and the classical Rossby-wave phase speed U_c, as well as a generalized form U_{cg} considering the generalized beta effect suggested by Theiss (2006).

Because stratifications are mostly surface intensified and the first baroclinic modes are dominant in the oceans, here we will only determine the classical and generalized Rhines effect for the first baroclinic mode. According to the classical dispersion relation of linear Rossby waves, the frequency of the first baroclinic Rossby waves can be denoted by

$$\omega = \frac{-\beta k}{K^2 + L_d^{-2}}, \tag{3}$$

where k is the zonal wave number, K is the total wave number, and L_d is the first baroclinic Rossby deformation radius. After using the long wave approximation, K^2 would be neglected in Eq. (3). Hence, we can obtain the classical Rossby-wave phase speed for the first baroclinic mode as

$$U_c = \left|\frac{\omega}{k}\right| = \beta L_d^2. \tag{4}$$

To assess the generalized Rhines effect considering the contributions of mean current and relative vorticity, Theiss (2006) proposed to use the generalized beta (β^*) instead of β when calculating the Rossby wave phase speed. The generalized beta can be expressed as

$$\beta^* = \beta - \frac{\partial^2 \bar{u}}{\partial y^2} + \frac{\bar{u}}{L_d^2}, \tag{5}$$

where $\bar{u}$ is the local time-mean zonal velocity. In fact, except for the term of horizontal shear, Eq. (5) is a simplified form of the mean quasi-geostrophic potential vorticity gradient calculated by Smith (2007) and Tulloch et al. (2009), when only considering the first baroclinic mode. Here, to calculate β^*, we will use the time-mean surface absolute geostrophic velocity provided by the SSALTO/DUACS and the AVISO to be a measure of $\bar{u}$. Also using the long-wave approximation, the critical Rossby-wave phase speed U_{cg} for determining the generalized Rhines effect can be calculated with β^* replacing β as

$$U_{cg} = \left|\beta^* L_d^2\right|. \tag{6}$$

To estimate U_c or U_{cg}, the first Rossby deformation radius L_d are also provided from the data calculated by Chelton et al. (1998). The characteristic eddy velocity scale U_e are estimated from the EKE field using Eq. (1).

Figures 2a and b show the geographical distribution of U_c–U_e and U_{cg}–U_e, respectively. The black dashed lines in the figures highlight the 0 isolines, where U_c=U_e or U_{cg}=U_e. When comparing these two figures with the global geographical distribution of eddies and their amplitudes given by Chelton et al. (2011) (Figs 5 and 10 therein), they both appear to replicate the general features described by Chelton et al. (2011), but Fig. 2b shows more consistent and detailed characteristics than Fig. 2a, especially in the mid-latitude oceans. In the tropical oceans, where Rossby waves dominate, the Rossby-wave phase speed U_c (U_{cg}) is much larger than the eddy scale velocity U_e, as shown in both Figs 2a and b. Outside the tropical regions, more consistently detailed features can be shown in Fig. 2b whereas only negative values are found in Fig. 2a. Comparing Fig. 2b with Figs 5 and 10 in Chelton et al. (2011), we can see a high consistency between the geographical characteristics shown, especially the two "eddy desert" regions surrounded by the 0 isolines of U_{cg}–U_e, as reported by Chelton et al. (2007). Hence, hereafter we will only discuss the generalized Rhines effect on the geographical eddy distributions.

From Fig. 2b, in the regions where $U_e > U_{cg}$, more and larger eddies were detected by the altimeters, also shown in the figures of Chelton et al. (2011). On the contrary, in those regions with positive values, where $U_e \leqslant U_{cg}$, fewer or even no eddies could be detected and hence "eddy deserts" formed. These features are

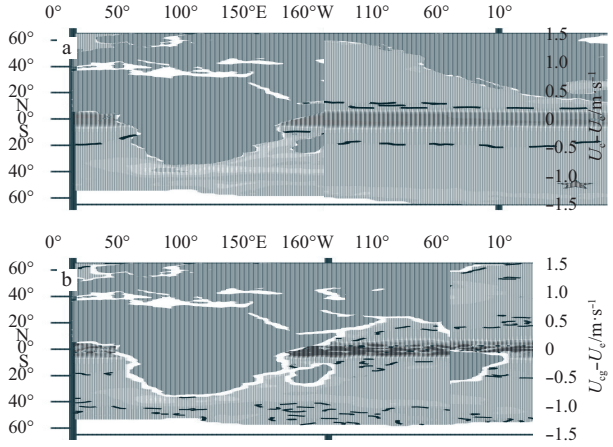

Fig. 2. Global map of U_c–U_e (a) and U_{cg}–U_e (b). The dashed blank lines denote 0 isolines and the core position of the two eddy deserts reported by Chelton et al. (2007) are denoted as pentagrams.

consistent with our argument for the eddy growth and destruction described in the previous section. Figure 2b also shows several other "eddy desert" regions ($U_e \leqslant U_{cg}$), except the two first reported by Chelton et al. (2007), which lie mostly in ACC regions, as well as along the main streams of the west boundary current in the Northern Hemisphere such as the Kuroshio and the Gulf Stream.

To further quantitatively examine the Rhines effect on the geographical characteristics of the altimeter-observed eddies, we also used various statistical data, such as eddy number, eddy amplitude, and eddy size, calculated by Chelton et al. (2011), as well as the maximum magnitude of the inverse KE cascade data obtained by Wang et al. (2015) to discuss the relationship between U_{cg}–U_e and eddy geographical characteristics.

Figure 3 shows the altimeter-observed eddy number, amplitude, growth ratio, and the maximum magnitude of the inverse KE cascade against the speed difference (U_{cg}–U_e). The eddy growth ratio is defined as the ratio of the difference between the observed eddy size and the local first baroclinic Rossby radius to the local Rossby radius, for which only positive values are plotted. The reason for using the eddy growth ratio instead of the eddy size is to suppress the influence of the local baroclinic Rossby radius on the altimeter-observed eddy size. The maximum magnitude of the inverse KE cascade can indicate the local strength of the upscale KE transfer associated with the eddy growth, where the Rhines scale is larger than the local first Rossby radius (see details in Wang et al. (2015)). All of the data are compared in each 1°×1° box identical to the statistical eddy data given by Chelton et al. (2011). Here, only eddy data with a lifetime larger than 16 weeks are plotted.

From Fig. 3, we can see that the regions with the largest eddy amplitudes and more detected eddies lie mostly in the regions where $U_e > U_{cg}$. In the regions of $U_e \leqslant U_{cg}$, the eddy amplitudes are mostly smaller than 10 cm and very few are larger than 15 cm. Similarly, there are typically fewer than ten eddies in those areas, and seldom more than 20. Overall, the regions where $U_e > U_{cg}$ occupy 73.7% of the global ocean area that has valid data. The growth ratios of the eddy sizes show a similar distribution to that of the eddy amplitude or quantity. The tails at the bottom right of the distributions in Figs 3a to c, located where $U_e \leqslant U_{cg}$, mostly lie in tropical regions (approximately 78%) and the rest (approximately 22%) are located in the "eddy deserts" outside of the tropical oceans. The inverse energy cascade also occurs mostly in the regions where $U_e > U_{cg}$, consistent with the distribution of eddy growth ratios. Generally, the regions where the speed difference (U_{cg}–U_e) is larger also have stronger inverse KE cascade magnitudes.

4 Discussion and summary

In order to better understand the formation mechanism of the "eddy desert" first reported by Chelton et al. (2007), in this short report, we examined a generalized form of the Rhines effect, suggested by Theiss (2006), on the geographical characteristics of the altimeter-observed eddies by comparing an U_e and an U_{cg}, which have considered the generalized beta effect.

Our argument is that, when $U_e \leqslant U_{cg}$, eddies can be easily deformed by Rossby waves and cease to grow. For the opposite situation (when $U_e > U_{cg}$), eddies may continue to develop via an inverse KE cascade and grow large enough to be detected by altimeters.

Our results show that the generalized Rhines effect has a much greater influence on the global geographical distribution of

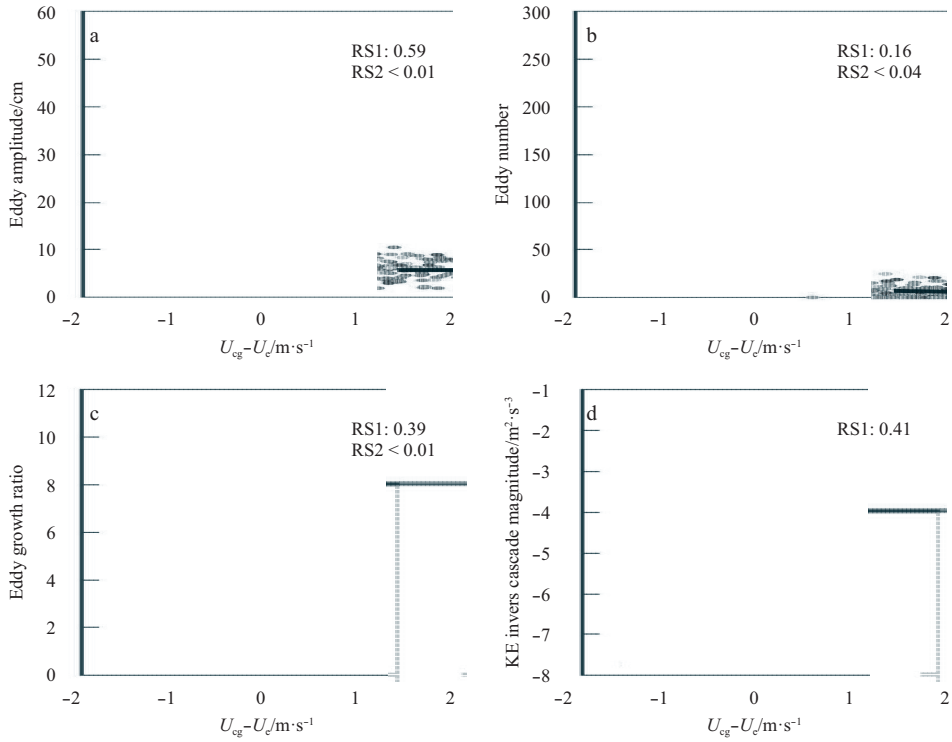

Fig. 3. Eddy statistical characteristics. The eddy amplitude (a), eddy number (b), eddy growth ratio (c), and logarithm of maximum magnitude of the inverse KE cascade (d) via U_{cg}–U_e. The linear polyfit curves for U_{cg}–U_e<0 and U_{cg}–$U_e \geqslant 0$ (except for Fig. 3d) are plotted as solid and dash lines, respectively. The R-squared values for each solid (RS1) and dashed (RS2) polyfit lines are marked in each figure.

the altimeter-observed eddies than the classical Rhines effect that considers the simple beta effect due to only the meridional gradient of the planetary vorticity. The largest amount of eddies are detected in the regions where $U_e > U_{cg}$, in which eddies can grow by the inverse KE cascade and have much larger amplitudes and sizes. The "eddy desert" regions outside of the tropical oceans, in which eddies exist in much lower quantities with much weaker amplitudes, lie in the areas where $U_e \leqslant U_{cg}$, illustrated clearly by the 0 isolines of U_{cg}–U_e.

Hence, the generalized Rhines effect also can be regarded as a "separation mechanism", which can clearly separate the zones where are wave-dominated or eddy (turbulence)-dominated by the isolines of U_{cg}–U_e. The wave-dominated areas, in which eddies could be easily destroyed by Rossby waves, form those regions of "eddy desert".

It should be noted that our analysis has assumed that the baroclinic instability is the main mechanism to generate eddies, while Stammer and Wunsch (1999) shows that the wind power input may play crucial roles for eddy activities in the north Pacific (near the eddy desert region in the north Pacific) and the subpolar north Atlantic, shown as their Fig. 18. Whether the high wind power input in those regions has any relationship with the formation of "eddy desert" is not clear yet and beyond the scope of this article, which should be studied further in the future.

Acknowledgements

The authors thank the three anonymous reviewers for help with improving the manuscript and Berloff P. for a helpful discussion on this subject. The altimeter products are produced by the data unification and altimeter combination system (DUACS) and AVISO which can be downloaded from ftp.aviso.oceanobs.com. The eddy statistical data, such as eddy number, eddy amplitude, and eddy size calculated by Chelton et al. (2011), can be downloaded from http://cioss.coas.oregonstate.edu/eddies/nc_data.html. The global first baroclinic Rossby radius data, calculated by Chelton et al. (1998), can be downloaded from http://www-po.coas.oregonstate.edu/research/po/research/ rossby_radius/. The maximum magnitude of the inverse KE cascade data were calculated and presented by Wang et al. (2015).

References

Charney J G. 1947. The dynamics of long waves in a baroclinic westerly current. Journal of Meteorology, 4(5): 135–162

Chelton D B, deSzoeke R A, Schlax M G, et al. 1998. Geographical variability of the first baroclinic rossby radius of deformation. Journal of Physical Oceanography, 28(3): 433–460

Chelton D B, Schlax M G, Samelson R M, et al. 2007. Global observations of large oceanic eddies. Geophysical Research Letters, 34(15): L15606

Chelton D B, Schlax M G, Samelson R M. 2011. Global observations of nonlinear mesoscale eddies. Progress in Oceanography, 91(2): 167–216

Chemke R, Kaspi Y. 2015. The latitudinal dependence of atmospheric jet scales and macroturbulent energy cascades. Journal of the Atmospheric Sciences, 72(10): 3891–3907

Chemke R, Kaspi Y. 2016. The latitudinal dependence of the oceanic barotropic eddy kinetic energy and macroturbulence energy transport. Geophysical Research Letters, 43(6): 2723–2731

Eady E. 1949. Long waves and cyclone waves. Tellus, 1(3): 33–52

Ferrari R, Wunsch C. 2009. Ocean circulation kinetic energy: reservoirs, sources, and sinks. Annual Review of Fluid Mechanics, 41(1): 253–282

Galperin B, Sukoriansky S, Dikovskaya N, et al. 2006. Anisotropic turbulence and zonal jets in rotating flows with a β-effect. Nonlinear Processes in Geophysics, 13(1): 83–98

Galperin B, Sukoriansky S, Dikovskaya N. 2010. Geophysical flows with anisotropic turbulence and dispersive waves: flows with a β-effect. Ocean Dynamics, 60(2): 427–441

Gill A E, Green J S A, Simmons A J. 1974. Energy partition in the large-scale ocean circulation and the production of mid-ocean eddies. Deep Sea Research and Oceanographic Abstracts, 21(7): 499–528

Holloway G, Hendershott M C. 1977. Stochastic closure for nonlinear Rossby waves. Journal of Fluid Mechanics, 82(4): 747–765

Pascual A, Faugère Y, Larnicol G, et al. 2006. Improved description of the ocean mesoscale variability by combining four satellite altimeters. Geophysical Research Letters, 33(2): L02611

Phillips N A. 1954. Energy transformations and meridional circulations associated with simple baroclinic waves in a two-level, quasi-geostrophic model. Tellus, 6(3): 273–286

Qiu Bo, Chen Shuiming, Klein P, et al. 2014. Seasonal mesoscale and submesoscale eddy variability along the North Pacific Subtropical Countercurrent. Journal of Physical Oceanography, 44(12): 3079–3098

Luo D, Zhong L, Franzke C. 2015. Inverse Energy Cascades in an Eddy-Induced NAO-Type Flow: Scale Interaction Mechanism. Journal of the Atmospheric Sciences, 72(9): 3417–3448

Rhines P B. 1975. Waves and turbulence on a beta-plane. Journal of Fluid Mechanics, 69(3): 417–443

Sasaki H, Klein P, Qiu Bo, et al. 2014. Impact of oceanic-scale interactions on the seasonal modulation of ocean dynamics by the atmosphere. Nature Communications, 5: 5636, doi: 10.1038/ncomms6636

Scott R B, Wang Faming. 2005. Direct evidence of an oceanic inverse kinetic energy cascade from satellite altimetry. Journal of Physical Oceanography, 35(9): 1650–1666

Smith K S. 2004. A local model for planetary atmospheres forced by small-scale convection. Journal of Atmospheric Sciences, 61(12): 1420–1433

Smith K S. 2007. The geography of linear baroclinic instability in Earth's oceans. Journal of Marine Research, 65(5): 655–683

Stammer D. 1997. Global characteristics of ocean variability estimated from regional TOPEX/POSEIDON altimeter measurements. Journal of Physical Oceanography, 27(8): 1743–1769

Stammer D, Wunsch C. 1999. Temporal changes in eddy energy of the oceans. Deep Sea Research Part II: Topical Studies in Oceanography, 46(1-2): 77–108

Sukoriansky S, Dikovskaya N, and Galperin B. 2007. On the arrest of inverse energy cascade and the Rhines scale. Journal of the Atmospheric Sciences, 64(9): 3312–3326

Theiss J. 2004. Equatorward energy cascade, critical latitude, and the predominance of cyclonic vortices in geostrophic turbulence. Journal of Physical Oceanography, 34(7): 1663–1678

Theiss J. 2006. A generalized Rhines effect and storms on Jupiter. Geophysical Research Letters, 33(8): L08809

Tulloch R, Marshall J, Smith K S. 2009. Interpretation of the propagation of surface altimetric observations in terms of planetary waves and geostrophic turbulence. Journal of Geophysical Research: Oceans, 114(C2): C02005, doi: 10.1029/2008JC005055

Tulloch R, Marshall J, Hill C, et al. 2011. Scales, growth rates, and spectral fluxes of baroclinic instability in the ocean. Journal of Physical Oceanography, 41(6): 1057–1076

Vallis G K, Maltrud M E. 1993. Generation of mean flows and jets on a beta plane and over topography. Journal of Physical Oceanography, 23(7): 1346–1362

Wang shihong, Liu Zhiliang, Pang Chongguang. 2015. Geographical distribution and anisotropy of the inverse kinetic energy cascade, and its role in the eddy equilibrium processes. Journal of Geophysical Research: Oceans, 120(7): 4891–4906

Williams G P. 1978. Planetary circulations. I - Barotropic representation of Jovian and terrestrial turbulence. Journal of the Atmospheric Sciences, 35(8): 1399–1426

Wunsch C. 1997. The vertical partition of oceanic horizontal kinetic energy. Journal of Physical Oceanography, 27(8): 1770–1794